Chemical Distribution and Bonding of Lithium in Intercalated Graphite: Identification with Optimized Electron Energy Loss Spectroscopy

ARTICLE *in* ACS NANO · FEBRUARY 2011

Impact Factor: 12.88 · DOI: 10.1021/nn1028168 · Source: PubMed

7 AUTHORS, INCLUDING:

Feng Wang
Brookhaven National Laboratory
46 PUBLICATIONS **966** CITATIONS
SEE PROFILE

Mario Sergio Moreno
Centro Atómico Bariloche
82 PUBLICATIONS **1,084** CITATIONS
SEE PROFILE

Lijun Wu
Brookhaven National Laboratory
143 PUBLICATIONS **2,921** CITATIONS
SEE PROFILE

Vyacheslav V Volkov
Brookhaven National Laboratory
105 PUBLICATIONS **971** CITATIONS
SEE PROFILE

Chemical Distribution and Bonding of Lithium in Intercalated Graphite: Identification with Optimized Electron Energy Loss Spectroscopy

Feng Wang,[†] Jason Graetz,[†] M. Sergio Moreno,[‡] Chao Ma,[†] Lijun Wu,[†] Vyacheslav Volkov,[†] and Yimei Zhu*[,†]

[†]Brookhaven National Laboratory, Upton, New York 11973, United States, and [‡]Centro Atómico Bariloche, San Carlos de Bariloche, 8400, Argentina

ABSTRACT Direct mapping of the lithium spatial distribution and the chemical state provides critical information on structure-correlated lithium transport in electrode materials for lithium batteries. Nevertheless, probing lithium, the lightest solid element in the periodic table, poses an extreme challenge with traditional X-ray or electron scattering techniques due to its weak scattering power and vulnerability to radiation damage. Here, we report nanoscale maps of the lithium spatial distribution in electrochemically lithiated graphite using electron energy loss spectroscopy in the transmission electron microscope under optimized experimental conditions. The electronic structure of the discharged graphite was obtained from the near-edge fine structure of the Li and C K-edges and *ab initio* calculations. A 2.7 eV chemical shift of the Li K-edge, along with changes in the density of states, reveals the ionic nature of the intercalated lithium with significant charge transfer to the graphene sheets. Direct mapping of lithium in graphite revealed nanoscale inhomogeneities (nonstoichiometric regions), which are correlated with local phase separation and structural disorder (*i.e.*, lattice distortion and dislocations) as observed by high-resolution transmission electron microscopy. The surface solid−electrolyte interphase (SEI) layer was also imaged and determined to have a thickness of 10−50 nm, covering both edge and basal planes with LiF as its primary inorganic component. The Li K-edge spectroscopy and mapping, combined with electron microscopy-based structural analysis provide a comprehensive view of the structure-correlated lithium intercalation in graphite and of the formation of the SEI layer.

KEYWORDS: lithium batteries · electron energy loss spectroscopy · transmission electron microscopy · graphite · lithium K-edge · *ab initio* calculations

Lithium batteries are the most popular rechargeable storage devices used in portable electronics and will likely be the primary power source for electrical vehicles in the near future.[1] Graphite is well suited as anode material for lithium batteries due to its low potential relative to lithium metal and its well-defined layered structure that permits reversible lithium intercalation. When paired with the appropriate electrolyte, the formation of a thin solid−electrolyte interphase (SEI) layer on the surface protects the material from solvent cointercalation. Various dynamics studies suggest that lithium is either intercalated into graphite or deposited onto edge planes.[2] It is commonly accepted that the first plateau in the discharge curve (at ~0.6 eV) indicates the formation of the SEI layer generated from the reaction of lithium with the electrolyte. Because of its critical importance in determining battery performance, characterization of the structure (*e.g.*, thickness and porosity) and composition of the SEI layer at high spatial resolution have been the subject of intensive studies.[3] There is great interest in understanding lithium transport, especially in nanostructured materials where boundaries and interfaces are abundant.[4,5] Recently, Balke *et al*. used atomic force microscopy (AFM), with its high sensitivity to the volume change, to obtain spatial variation of the lithium diffusion at a submicrometer scale that is artificially created by applying a high voltage bias.[6] However, the direct observation of lithium electrochemically intercalated into electrode materials has remained elusive. High-resolution transmission electron microscopy (TEM) can routinely resolve individual atomic columns of graphite; nevertheless resolving individual Li atoms or Li columns is much more challenging.[7,8] Electron energy loss spectroscopy carried out in the TEM (TEM-EELS) is in principle appropriate for spectroscopy and mapping of lithium because of the high ionization cross-section of the shallow Li K-edge, which is 10−100 times greater than that of other light elements, such as O and F. Instead of directly imaging individual Li columns by HRTEM, where a high beam current over a small area causes rapid radiation damage, Li mapping with TEM-EELS can be performed at lower magnifications with less current density (lower dose rate). In addition, the near-edge fine structure of the Li K-edge provides information on the electronic environment of the Li atoms in the graphite and allows us to differentiate between various lithium species.[9]

*Address correspondence to zhu@bnl.gov.

Received for review October 19, 2010 and accepted December 17, 2010

Published online January 10, 2011
10.1021/nn1028168

Understanding of the composition and formation of the SEI layer is still one of the grand challenges in lithium battery research, despite three decades of efforts.[2,10,11] The chemical composition of the SEI layer depends on many factors, including electrolyte content (solvent, salts, additives, and impurities) and reaction conditions.[12] It is generally believed that the SEI layer is comprised of reduction products with both inorganic and organic species.[13] However, a detailed composition of the SEI on carbonaceous anodes cycled in nonaqueous electrolytes has not been well established, and some reports show the presence of Li_2CO_3 and Li_2O in the SEI,[14] while others do not.[13,15]

Various analytical tools have been used to study the complex SEI layer, each with its advantages and limitations. For example, X-ray photoelectron spectroscopy (XPS) identified lithium halides (*e.g.*, LiF) as the main component of the SEI formed on the edge plane of the graphite, but they were hardly detectable with Fourier transform infrared spectroscopy (FTIR), which is better at detecting surface organic species. Usually, information from different characterization methods must be combined to resolve all possible components of the intricate SEI layer. Importantly, the SEI is highly sensitive to moisture and oxygen, and reliable results require special experimental designs that minimize or eliminate exposure to air. Recent experiments explored the lateral distribution of SEI components and the composition of the edge/basal planes of highly oriented pyrolytic graphite (HOPG) *via* time-of-flight secondary ion mass spectrometry (TOF-SIMS) and XPS; however, the spatial resolution of these techniques is limited to 1 μm.[16] Despite its advantage in spatial resolution, TEM-EELS has scarcely been utilized for studying the SEI layer.[17]

Given the low mass of Li, radiation damage *via* radiolysis and sputtering prohibits the spectroscopy and mapping of lithium in its pristine state. It is critical to identify how damage occurs and the products of beam damage and, most importantly, to optimize the experimental conditions for achieving the highest possible spatial solution while minimizing beam damage. Plural inelastic scattering by plasmon excitation is another special concern when measuring the Li K-edge due to its proximity to the low-energy plasmon region. Double plasmon scattering distorts the pre-edge background and can mask the Li K-edge, especially in thick samples where multiple scattering is prevalent. Artifacts due to plural scattering can be reduced by increasing the inelastic mean-free-path or restricting analyses to thin regions of the sample. In addition to these needed technical requirements for high-quality Li K-edge spectra, the demands of quantitatively interpreting the Li K-edge structure to obtain information on bonding and electronic structure are daunting.

In this study, we investigated the origins of electron-induced beam damage in lithium-containing materials and established optimal conditions to minimize radiation damage and plural scattering. We recorded reference Li K-edge spectra from a series of lithium standards (*e.g.*, Li, LiF, $LiPF_6$, LiOH, Li_2O, and Li_2CO_3) and used them as "fingerprints" to identify the different lithium species in the bulk and on the surface (*e.g.*, SEI). We mapped the Li distribution by Li K-edge and determined the electronic structure of lithiated graphite from the near-edge fine structure in combination with *ab initio* calculations. The structure-correlated lithium intercalation into graphite and the formation of the SEI layer are discussed.

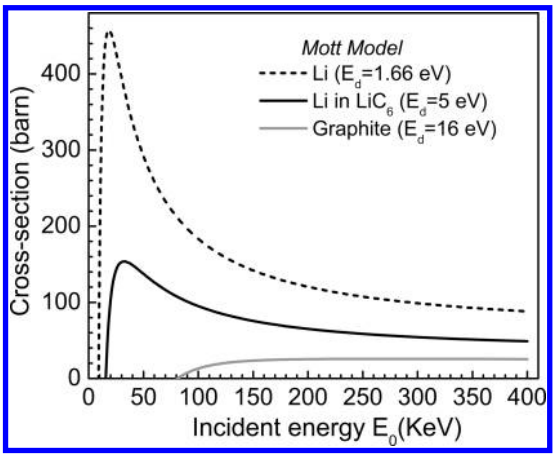

Figure 1. Calculated displacement cross-sections for lithium atoms in the elemental Li (black dashed line) and for lithiated graphite, LiC_6, (black solid line) and graphite (gray solid line) as a function of incident electron energy E_0 (KeV). TEM is generally operated between 80 and 400 KeV; low-kV (*i.e.*, 60 keV) TEM has been recently developed for studies of materials composed of light elements. We show here, however, for Li, 60 keV operation causes more damage than 300 keV.

RESULTS AND DISCUSSION

Electron Energy Loss Spectroscopy for Li-Containing Materials. Radiation damage in the TEM, *via* radiolysis or sputtering, is a major concern in studying lithium-containing materials. In metallic or covalently bonded materials, radiolysis is quenched quickly due to the availability of free electrons. In this case, sputtering, mainly in the form of knock-on displacement from high-angle elastic scattering, is often the primary cause of beam damage.[18,19] Lithium and lithium-intercalated graphite (*i.e.*, metallic LiC_6) are extremely susceptible to sputtering damage because of their small nuclear mass. The sputtering cross-section can be evaluated using the Rutherford or Mott model[18,20] (details on the two different models are provided in the Supporting Information).

Figure 1 shows the calculated sputtering cross-sections for lithium atoms in the elemental state and for lithiated graphite (LiC_6) and carbon atoms in the graphite as a function of the incident energy E_0. Conventional wisdom suggests that a low TEM operating voltage ($\leq$100 kV) is optimal for reducing radiation damage; but our calculations demonstrate that this is not true for

lithium and lithium compounds. The displacement cross-section for elemental Li is high at low voltages and reaches maximum at as low as 18 keV. The displacement energy, E_d, is higher for Li atoms in lithiated graphite (LiC_6), and the cross-section reaches a maximum at around 32 keV and then decreases with accelerating voltage. This surprising behavior is due to the small nuclear mass of Li, which makes it easily displaced by fast incident electrons at relatively low voltage, where the elastic scattering cross-section is high. As expected, these calculations (Figure 1) show that the displacement cross-sections for Li are much larger than that for graphite, the latter being much smaller and increasing slowly with incident voltage. It should be noted that carbon atoms in graphite have a much higher displacement energy and an overall different behavior from that of amorphous carbon (E_d = 8 eV).[18] Based on these results, the optimal accelerating voltage for TEM studies of LiC_6 is around 300 kV, where the cross-sections for Li and carbon atoms are both low. Since the knock-on threshold for elemental Li is 9 kV (15 kV in LiC_6), our study suggests aberration-corrected low-voltage (40−80 kV) electron microscopes recently under development for imaging light elements may not be suitable for studying lithium ion batteries.

Unlike LiC_6, which is primarily susceptible to sputtering damage, the complex SEI is composed of both organic and insulating inorganic lithium compounds; damage mostly occurs through radiolysis arising from various ionization or excitation processes. It should be noted that radiolysis is more efficient than sputtering damage since the cross-section is about 2−3 orders of magnitude higher than that of displacement. The energy loss near-edge fine structure (ELNES) of Li K-edge can be used as a "fingerprint" for phase identification; however, radiation dose should be low enough to ensure that the region of interest is not destroyed or transformed under the electron beam. The electron excitation cross-section is inversely proportional to the incident energy (Bethe theory)[21] and, therefore, operating the TEM at a higher voltage may be also favorable for reducing beam damage (although some contrast loss is expected). It is assumed that cryogenically cooled samples suffer less radiolysis damage, but this has never been verified and is unlikely. Radiolysis involves the fracture of bonds, which is indeed temperature independent. Although migration of atomic species slows down at cryogenic temperatures, damage (in the form of broken bonds) still occurs and becomes more apparent as the sample is warmed to room temperature. In our study, an accelerating voltage of 300 kV and operation of TEM at room temperature were chosen for all spectroscopy and lithium mapping. Sample heating due to electron beam irradiation is negligible when the beam is spread over a large area, and little temperature increase (below 1K) is expected in our TEM samples.[22]

Figure 2 shows the Li K-edge spectra for the fully lithiated graphite (LiC_6), elemental Li, and other Li compounds. The ELNES of the Li K-edge (*e.g.*, edge position and peak amplitude) varies considerably between different compounds, reflecting the different electronic environments of the central Li atoms. The Li K-edge from LiC_6 was recorded from fully lithiated graphite, with a momentum (k) parallel to the c-axis ($k//c$). A chemical shift of about 2.7 eV, with respect to elemental Li, is observed in the Li K-edge from LiC_6 (57.5 eV; top curve in Figure 2). This result is consistent with other measurements and indicates charge transfer from the intercalated Li to the graphene sheets.[23−25]

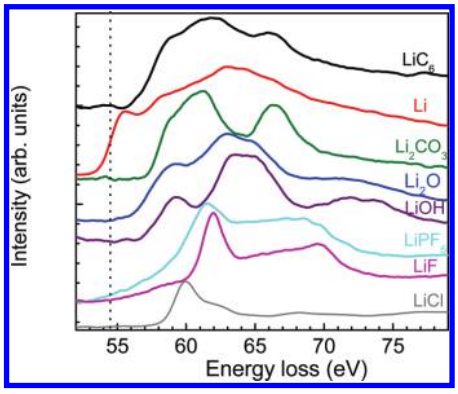

Figure 2. Experimentally measured Li K-edge near-edge fine structure for a series of lithium compounds, *viz.*, Li, LiC_6, Li_2CO_3, Li_2O, LiOH, $LiPF_6$, LiF, and LiCl. The Li K-edge threshold E_{th} is defined as the energy position at the half height of the edge jump; the vertical dotted line denotes the Li K-edge threshold for elemental Li (54.8 eV).

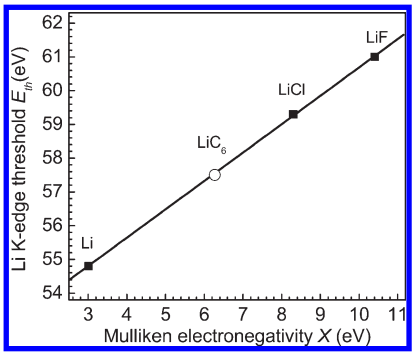

Figure 3. Edge threshold energies for elemental Li, LiC_6, LiF, and LiCl *versus* Mulliken electronegativity. The line shows the linear fit to the plot for Li, LiCl, and LiF (solid cubic); the data for LiC_6 (hollow circle) was not included in the fit.

Figure 3 is a plot of the measured Li K-edge threshold E_{th} *versus* the Mulliken electronegativity for Li, LiF, and LiCl; electronegativity is defined as the mean of the ionization potential and the electron affinity. An empirical relationship was established relating the onset energy of the Li K-edge to the electronegativity, X, or equivalently, to the binding energy of the Li 1s electron. The relationship is linear and has the following form:

$$E_{th} = E_0 + k \cdot X \quad (1)$$

where the slope (k) is 0.84, and the onset energy (E_0) is 52.3 eV. A large chemical shift in the Li K-edge is observed in the lithium halides and can be attributed to the enhanced binding of the K-shell electrons as the

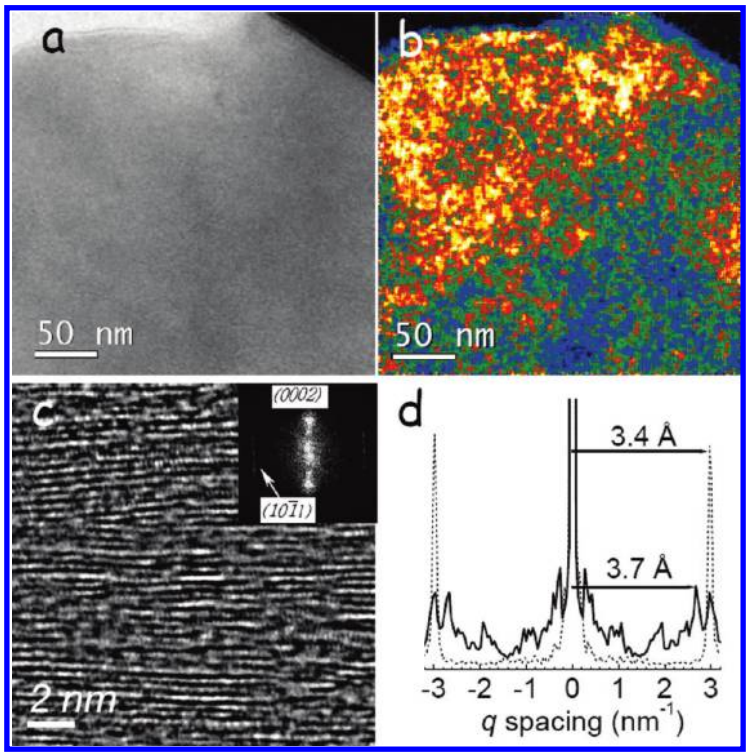

Figure 4. The local nonstoichiometric Li intercalation in the discharged graphite by BF TEM image (a) viewed along the [0001] zone axis and by corresponding false-color (using temperature scale) Li concentration map (b), in a combination with HRTEM images viewed along [11−20] zone axis (c). The plot (d) for the vertical intensity profile from (000−2) to (0002) reflection in the FFT inset in (c), in which the thin dashed curve is for the pristine graphite and the thick solid curve for the lithiated graphite. The inner calibrations were made for HRTEM images by reference to a common d_{10-10} = 2.13 Å spacing. The dark contrast in the upper-right corner in images (a, b) is due to the thick carbon support of the TEM grid.

L-shell electrons are pulled to anion sites. The Li K-edge onset in LiC_6 follows the same relationship, suggesting that Li in LiC_6 has a similar ionic character. The nature of the bonding between the Li and the graphite host is further discussed below in accordance with the electronic structure studies.

The Li K-edge of $LiPF_6$ is similar to that of LiF, but the features are broader and the edge position of $LiPF_6$ is about 0.5 eV lower than that of LiF. The distinct features in the ELNES of the Li K-edge for Li_2CO_3, Li_2O and LiOH are also shown in Figure 2. There is a limited amount of EELS data in the literature, and even among these, the fine spectral features of the Li K-edge often vary widely due to differences in instrumental resolution and operating conditions.[26] A recent report on the Li K-edge from electrochemically lithiated graphite shows a featureless near-edge region possibly because the spectra were recorded from a large area, averaged over different graphite orientations, and also partially due to contributions from SEI compounds.[27]

Local Nonstoichiometric Li Intercalation in Fully Discharged Graphite. In this experiment, the incident beam is parallel to the *c*-axis of the graphite (namely *B* = [0001]). Very weak diffraction contrast is present in the bright-field (BF) TEM image as shown in Figure 4a. To obtain the Li concentration map, the Li elemental map and the thickness map (not shown here) were recorded from the same area. In this selected area, the graphite is very uniform in thickness (of 40−50 nm) over the whole field of view. Small variation in the thickness was corrected pixel-by-pixel; in addition, 300 kV electrons were used to reduce the influence of plural scattering. Accordingly, the resulting lithium concentration map in Figure 4b represents the real distribution of Li in the graphite independent of the sample thickness. The variation in local Li concentration is illustrated by the relative color change at a temperature scale spanning from dark blue, representing little/no Li, to bright yellow, representing a high Li concentration. Clearly the Li concentration is higher in the areas closer to the edge but lower in the areas away from the edge. Locally, small Li-rich domains (5−10 nm) are surrounded by Li-poor areas.

The nanoscale inhomogeneities in the Li intercalated graphite may also be indirectly learned from the structure analysis, since graphite at different states of lithiation is correlated with the lattice expansion in the *c*-direction in the HRTEM images. Figure 4c was recorded along the [11−20] direction (perpendicular to the *c*-axis). Over the full field of view, local abrupt changes of the lattice spacing are apparent from site to site. For quantitative *d*-spacing measurements we used the internal calibration based on common lattice spacing d_{10-10} = 2.13 Å that is not affected by lithium intercalation. Inhomogeneous Li intercalation results in nonuniformity

of the (0002) lattice spacing are clearly seen in the lattice image of Figure 4c. There is an intermixture of lattices with local spacing, $d_{0002} \approx 3.7$ Å (corresponding to graphite layer spacing in LiC_6), and those with a smaller spacing (corresponding to Li-poor phases, such as Li_xC_6 ($x < 1$)) over the full field of view. This may also be seen in the broadening of the fast Fourier transforms (FFT) pattern in the inset of Figure 4c. Similar HRTEM observations were also reported by Song *et al.*[28] Measurements of the d(0002) spacing in fully discharged graphite (Figure 4d) show two strong peaks with $d_{0002} \cong 3.7$ and 3.4 Å in the power spectrum, corresponding to fully intercalated (LiC_6) and nonlithiated (C); also there are two more broadened and weak peaks, corresponding to Li-poor phases ($Li_{2/3}C_6$ and $Li_{1/3}C_6$). This local multiphase distribution was not seen by the XRD examination of the full electrode (Figure S1, Supporting Information), in which peaks associated with primary LiC_6 and minor LiC_{12} phases were identified. However, the nonlithiated (C) phase and the other Li-poor phases $Li_{2/3}C_6$ and $Li_{1/3}C_6$ were not identified.

Li intercalation in principle leads to the change of the stacking sequence from ABAB in the pristine graphite to AAAA in the fully intercalated graphite (LiC_6). This phenomenon was hardly resolved in our observations because of abrupt variations in the stoichiometry of Li intercalation. However edge dislocations along (0002) planes are commonly observed, as indicated by oval circles in the inverse FFT images (Figure S2, Supporting Information). The results are similar to an early report on the existence of isolated dislocations in graphite intercalated with FeF_2.[29] Regions where the lattice has a uniform spacing (d_{0002} = 3.7 Å) are small and only a few nanometers in diameter. Importantly, the domains of the LiC_6 phase are directly correlated with the Li-rich domains revealed by the Li map in Figure 4b. Atomic defects, such as interstitial atoms and vacancies, are intrinsic in synthetic graphite. However, the large d_{0002} spacing of the graphite lattice, related to empty van der Waals gaps between atomic carbon layers, appears to be uniform across the sample, as demonstrated by the intensity profile in Figure 4d (dashed line). The large differences in the d_{0002} spacing are primarily due to nonuniform Li-intercalation that fills the van der Waals gaps in the layered graphite structure. The intercalation of lithium is likely affected by the presence of dislocations, which bounds the intercalated Li layers.

Electronic Structure of the Fully Discharged Graphite. The Li K-edge originates mainly from excitations of the Li 1s into the 2p orbital, and the difference in the near-edge fine structure (shown in Figure 2) reflects changes in the Li electronic environment. For a correlation of the spectral feature with electronic structure in the lithiated graphite, the density-of-states (DOS) projected onto Li and C sites and the corresponding near-edge fine structure were calculated by Wien2k and FEFF codes

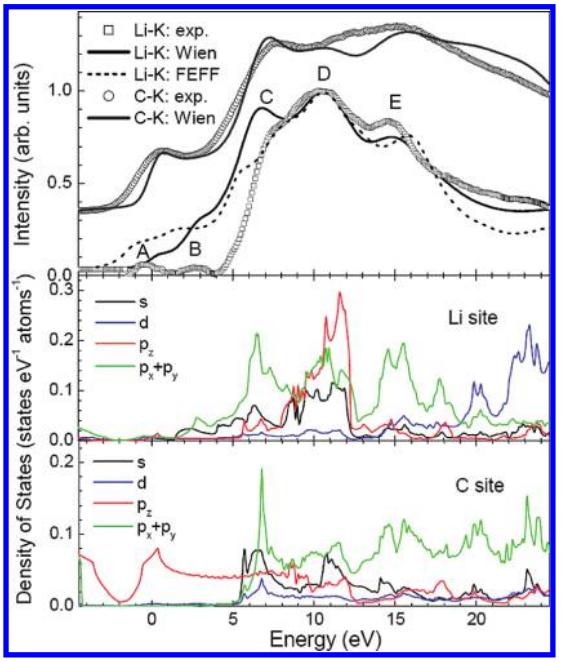

Figure 5. Calculation of the electronic structure and spectra of the fully discharged graphite (LiC_6) using Wien2k code against the experimental data for Li (hollow square) and C K-edges (hollow circle). FEFF calculation of the Li K-edge is also given (dot line) for comparison. Actual experimental conditions (collection angles, e-beam direction, and instrumentation broadening) were included in the calculations.

(details on the calculations are provided in the Supporting Information). The experimental and calculated results are presented in Figure 5. By taking experimental conditions into account, the calculation reproduces the main features of the experimentally measured Li and carbon K-edges very well. Also, calculations performed using the Wien2k and FEFF codes gave similar results. The energy positions of the Li and C K-edges were realigned with Fermi energy E_F (set to 0 eV). Above the threshold energy of the Li K-edge there are three intense peaks labeled as C, D, and E at 7.0, 10.4, and 14.9 eV respectively. Two extra weak peaks (labeled as A and B) at around 0.5 and 2.9 eV in the calculated spectrum may correspond to the two bumps in the experimental spectrum; however, their amplitude may be altered somewhat by the background subtraction.

The various features of the near-edge structure can be assigned to different excitations using the calculated, orientation-dependent spectra and the projected density of states (PDOS) toward different orbitals. As shown in the middle panel of Figure 5, the Li PDOS is dominantly contributed by the 2p and 3s states within 20 eV of E_F. The 2p states consist of three intense peaks of $p_x + p_y$ character located at 6.8, 11, and 15 eV above E_F and one intense peak of p_z character at 11.5 eV. Therefore, peaks C and E in the near-edge structure are primarily due to transitions into the in-plane $p_x + p_y$ orbital, while the broad D peak consists of two peaks from excitations into the in-plane $p_x + p_y$ and out-of-plane p_z orbitals.

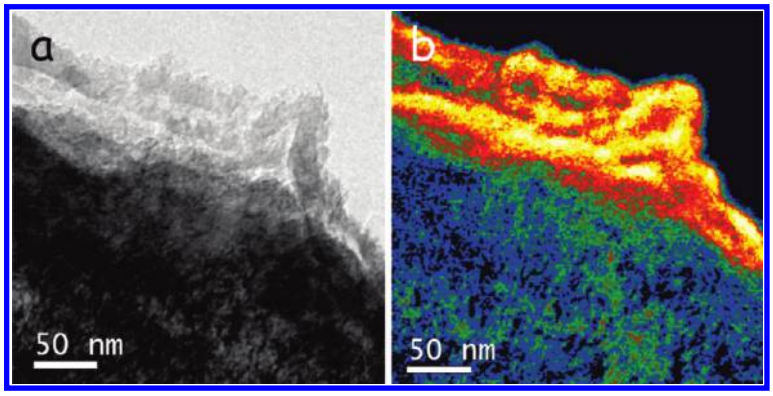

Figure 6. The morphology study of the solid electrolyte interphase of the graphite discharged to 10 mV and washed in the dimethyl carbonate by (a) BF TEM image and (b) Li concentration map, viewed along the [0001] zone axis.

The intercalation of Li into graphite leads to little change of the C K-edge, as shown in Figure 5 (top panel).[23,27] Similarly, calculations of electronic density of states reveal only subtle changes in the distribution of the C PDOS upon lithiation despite the stacking sequence change in the real space (Figure S5, Supporting Information). In contrast, the K-edge of intercalated Li exhibits a shift to higher energies (Figure 3) and a rich fine structure (not seen with elemental Li), which is attributed to the anisotropic distribution of the Li PDOS. These results clearly suggest that Li has a an ionic character in lithium intercalated graphite and is not metallic (neutral valence), as previously suggested.[27]

Surface SEI. Figure 6a and b shows the BF TEM image and the corresponding Li map from a disassembled lithiated graphite electrode. The graphite was oriented with its *c*-axis pointing out of the paper, as determined by electron diffraction. The surface of the electrode is covered with a layer of spongy material with a high concentration of lithium that is defined as the SEI. The porous nature of the SEI is attributed to the organic components, which may not be captured in the mapping because of their high beam sensitivity. The only detectable component of the SEI layer appears to be LiF, as judged by the shape of the Li K-edge spectra (black) in Figure 7. The Li mapping reveals that the SEI layer covers both edge and basal planes. The thickness varies but is roughly within a range of 10−50 nm, as typically observed in our experiments. But in reality the thickness depends on many factors, such as the nature of the graphite, electrolyte, cycling history, *etc.*[30] It is important to note that the surface of an unwashed electrode is often coated with residual electrolyte, which is different from the SEI layer in the composition and morphology. In the Supporting Information, we give an example of the TEM image and the corresponding Li map from an unwashed electrode (Figure S4, Supporting Information). It exhibits a much smoother, denser surface layer than the SEI layer presented on the washed electrode (Figure 6).

The near-edge structure of the Li K-edge is sensitive to the lithium electronic environment (as shown in Figure 2) and can be used to differentiate between various lithium chemical species. The Li K-edge from the SEI area (acquired within one second to reduce damage to the material) is shown in spectrum I of Figure 7 (black solid line). As apparent from these results, the primary component of the SEI on the edges and basal planes is LiF (no other lithium species were detected), consistent with the recent investigations by Abraham *et al.*[15] The LiF is formed from the decomposition of the $LiPF_6$ salt during lithiation.[31,32] Although previous reports have shown the presence of Li_2CO_3 and Li_2O in the SEI,[14] their characteristic features (shown in Figure 2) were not identified in our Li K-edge measurements. The only compound consistently observed in the SEI of graphite electrodes using an $LiPF_6$ salt is LiF, which was observed here and was commonly reported in XPS studies.[31,33] The uncertainty over the SEI composition may be partly due to the fact that the makeup of the surface layer is extremely sensitive to electrode and electrolyte composition (*e.g.*, solvents, salt, impurities), cycling history, and sample preparation (*e.g.*, air exposure).[30]

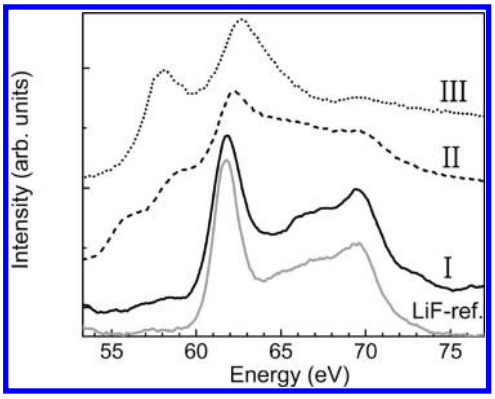

Figure 7. The Li K-edge spectra from the edge region in a comparison to that LiF. The spectra were recorded at different exposure: spectrum I was summed from 10 acquisitions at 0.1 s each (1 s total; black solid line), and spectrums II (black dashed line) and III (black dotted line) were acquired 1 and 10 min after spectrum I, respectively.

Radiation damage is an issue in studying lithium materials by TEM-EELS, and therefore, we have also investigated the change in the Li K-edge spectra from the SEI as a function of dose. Figure 7 shows that the

primary inorganic component of the SEI (*i.e.*, LiF) degrades very quickly under the electron beam, as evidenced by the change in the features of the Li K-edge. The appearance of shoulders at around 56 and 59 eV within 1 min of exposure points to the formation of elemental lithium. These lithium nanoparticles are quickly extruded out of the edge, as observed previously.[34] After approximately 10 min, a new phase has formed, which is identified as Li_2O from the formation of the two peaks at 58 and 62.5 eV. This is likely due to the reaction of the elemental Li with a small amount of residual oxygen or moisture in the TEM column that is further stimulated by exposure to the intense electron beam.[35] Therefore, the full beam damage process begins with the decomposition of the fluoride, engendering metallic lithium particles, and ultimately the formation of lithium oxide ($LiF \rightarrow Li \rightarrow Li_2O$). This is similar to what was previously reported for MgF_2,[35] demonstrating the importance of understanding radiation effects as a function of dose in using the fine structure as a fingerprint for identifying a particular species.

CONCLUSION

The spatial distribution and chemical states of lithium in electrochemically lithiated graphite were measured with nanometer resolution using TEM-EELS. The optimal experimental conditions were determined to mitigate radiation damage and plural scattering. Li K-edge spectra from a series of standards were used as "fingerprints", along with *ab inito* calculations, to identify the chemical species of lithium present on the surface and in the bulk electrode. The Li K near-edge fine structure and the calculated electronic DOS reveal the ionic nature of the intercalated lithium with significant charge transfer to the graphene sheets. For the first time, we demonstrate nonstoichiometric intercalation of Li at the nanometer scale in bulk graphite. In addition, the map of the SEI layer was obtained showing a 10−50 nm surface layer primarily composed of LiF. The high cross-section and the sensitivity of the Li K-edge to the Li electronic environment make TEM-EELS well suited to study Li transport and charge transfer in electrode materials for lithium batteries.

METHODS

Sample Preparation. TEM samples were prepared from electrochemically lithiated synthetic graphite. The as-received synthetic graphite (Alfa-Aesar) was coated onto a copper foil current collector and dried under dynamic vacuum at 120 °C for 8 h. Electrochemical cells (Hohsen, 2016 type) were prepared in an Ar glovebox using lithium metal as the counter electrode (half-cell) and a standard electrolyte of 1:1:1 ethylene carbonate (EC)/dimethyl carbonate (DMC)/$LiPF_6$. The cells were cycled electrochemically within the potential range of 1.5−0.01 V *versus* Li/Li^+ using an Arbin potentiostat. The cycling curves for the first five cycles are included in the Supporting Information (Figure S5). In studies of the fully lithiated graphite, the cells then were discharged to 10 mV at a current equivalent to C/20 and held at the voltage for 24 h to ensure that the electrodes were fully equilibrated; during this constant voltage period, the current typically dropped to approximately 1/10 of its initial value. In studies of the SEI layer, the cells were discharged to 10 mV at a current equivalent to C/20 to create a stable SEI layer on the surface.

The cycled cells were dissembled in the Ar glovebox, and the graphite electrodes were rinsed in DMC three times and dried under vacuum. Samples for X-ray diffraction were sealed under Ar using a thin kapton film to protect the electrode from air contamination. Small pieces of the graphite electrode were loaded onto the TEM lacey carbon grid and into a vacuum transfer holder, which was used to transfer the sample from an Ar glovebox into the TEM column without air exposure.

Characterization and Calculations. TEM-EELS spectra and images were recorded at 300 kV in the JEM-3000F microscope equipped with a Gatan image filter (GIF) spectrometer. The spectra were recorded in diffraction (image coupled) mode with an energy resolution of ~1.1 eV, as measured by the full width at half-maximum (fwhm) of the zero-loss peak (ZLP).

Several unique methods were used to increase the inelastic mean free path and reduce artifacts due to plural scattering in the energy loss images and spectra. First, the TEM was operated at a high accelerating voltage (300 kV), giving the electrons a long mean free path and resulting in less radiation damage to lithium. By taking advantage of the small characteristic angle, ~0.1 mrad for Li K-edge, small collection angles were used in both spectroscopy (semi-angle $\beta \sim 0.9$ mrad) and mapping (5.0 mrad) to lower the plasmon plural scattering; about 50% and 83% of the Li K-edge signal, respectively, were collected in spectroscopy and mapping. This also helps to reduce contributions from nondipole transitions, which become prevalent when the collection angle is large.[36]

We employed the three-window method for Li mapping, generating two images from the pre-edge and a third from the post-edge region. By fitting the pre-edge background intensity as an inverse-power function, its shape is allowed to vary across the image. This method is effective at removing plural scattering from pixel to pixel across the whole image. We selected only large areas with a uniform thickness and an orientation along the *c*-axis (determined by electron diffraction) for spectroscopy and mapping. For each lithium map, a thickness map was also recorded under the same conditions to check for possible artifacts arising from large variations in thickness. Finally, we used an energy window of 5.0 eV, the narrowest possible window to satisfy the required field of view.

Reference Li K-edge spectra were recorded under the same conditions for elemental Li and several Li standards (such as $LiPF_6$, LiF, Li_2O, Li_2CO_3, and LiOH). All samples were transferred from the glovebox into the TEM column *via* a high-vacuum transfer holder. Spectra were recorded with a spread beam to reduce beam damage. The energy positions of the Li K-edges were recalibrated in reference to the positions of the ZLP. The pre-edge background was fit to all spectra using a power law in the software Gatan Digital Micograph (version 1.81.78). An example of the background subtraction was given in Figure S6, Supporting Information.

To correlate the observed near-edge fine structure with the electronic structure of LiC_6, the Li and C K- edges were modeled by both full-potential method *via* the Wien2k code and the real-space full multiple-scattering (RSMS) calculations implemented in the FEFF code.[37,38] In both calculations, the EELS were calculated using relativistic cross-sections; actual experimental conditions, such as beam energy, collection semiangle, and beam orientation, were used in the calculations. Core-hole effects resulting from core-level excitation were treated using the final-state rule (FSR) or $z + 1$ approximation. Details on the calculations are given in the Supporting Information.

Supporting Information Available: Calculation details for near-edge fine structure and sputtering cross-section, cycling curve of the graphite, IFFT of the HRTEM image, XRD patterns for pristine and fully lithiated graphite, calculated DOS of the graphite and lithiated graphite, and TEM-EELS mapping of the unwashed lithiated graphite. This material is available free of charge *via* the Internet at http://pubs.acs.org.

Acknowledgment. Discussions with Prof. R. Egerton on EELS and radiation damage are gratefully acknowledged. This work was supported by the U.S. DOE under contract DE-AC02-98CH10886 with funding from Laboratory Directed Research and Development at Brookhaven National Laboratory. J.G. and F.W. were also supported by the Northeastern Center for Chemical Energy Storage, an Energy Frontier Research Center funded by the U.S. Department of Energy, Office of Basic Energy Sciences under award number DE-SC0001294. F.W. thanks NSERC of Canada for a fellowship. M.S.M. acknowledges partial financial support of CONICET (Argentina).

REFERENCES AND NOTES

1. Tarascon, J. M.; Armand, M. Issues and challenges Facing Rechargeable Lithium Batteries. *Nature* **2001,** *414*, 359–367.
2. Balbuena, P. B; Wang, Y. X. *Lithium-Ion Batteries: Solid-Electrolyte Interphases*; Imperial College Press: London. 2004.
3. Claye, A.; Fischer, J. E. Short-Range Order in Disordered Carbons: Where Does the Li Go? *Electrochim. Acta* **1999,** *45*, 107–120.
4. Arico, A. S.; Bruce, P.; Scrosati, B.; Tarason, J. M.; Schalkwijk, W. Nanostructured Materials for Advanced Energy Conversion and Storage Devices. *Nat. Mater.* **2005,** *4*, 366–377.
5. Armand, M.; Tarascon, J. M. Building Better Batteries. *Nature* **2008,** *45*, 652–657.
6. Bulke, N.; Jesse, S.; Morozovska, A. N.; Eliseev, E.; Chung, D. W.; Kim, Y.; Adamczyk, L.; Garcia, R.e.; Dudney, N.; Kalinin, S. V. Nanoscale Mapping of Ion Diffusion in a Lithium-Ion Battery Electrode. *Nat. Nanotech.* **2010,** 5749–754.
7. Shao-Horn, Y.; Croguennec, L.; Delmas, C.; Nelson, E. C.; O'Keefe, M. A. *Nat. Mater.* **2003,** *2*, 464–467.
8. Ross, M. D.; Erni, R.; Asta, M.; Radmilovic, V.; Dahmen, U. Atomic-Resolution Imaging of Lithium in Al3Li Precipitates. *Phys. Rev. B: Condens. Matter Mater. Phys.* **2009,** *80*, 024110(1−6).
9. Egerton, R. F. *Electron Energy Loss Spectroscopy in the Electron Microscope*, 2nd ed.; Plenum: New York, 1996.
10. Peled, E. J. The Electrochemical Behavior of Alkali and Alkaline Earth Metals in Nonaqueous Battery Systems-The Solid Electrolyte Interphase Model. *Electrochem. Soc.* **1979,** *126*, 2047–2051.
11. Goodenough, J. *et. al. Basic Research Needs for Electrical Energy Storage: Report of the Basic Energy Science Workshop on Electrical Energy Storage*; U.S. Department of Energy: Washington, DC, 2007.
12. Bryngelsson, H.; Stjerndahl, M.; Gustafsson, T.; Edstrom, K. How Dynamic is the SEI? *J. Power Sources* **2007,** *174*, 970–975.
13. Herstedt, M.; Andersson, A. M.; Rensmo, H.; Siegbahn, H.; Edstrom, K. Characterization of the SEI Formed on Natural Graphite in PC-based Electrolytes. *Electrochem. Acta* **2004,** *49*, 4939–4947.
14. Aurbach, D.; Markovsky, B.; Weissman, I.; Levi, E.; Ein-Eli, Y. On the Correlation between Surface Chemistry and Performance of Graphite Negative Electrodes for Li Ion Batteries. *Electrochem. Acta.* **1999,** *45*, 67–86.
15. Xiao, A.; Yang, L.; Lucht, B. L.; Kang, S. H.; Abraham, D. P. Examining the Solid Electrolyte Interphase on Binder-Free Graphite Electrodes. *J. Electrochem. Soc.* **2009,** *156*, A318–327.
16. Peled, E.; Tow, D. B.; Merson, A.; Gladkich, A; Burstein, L.; Golodnitsky, D. Composition, Depth Profiles and Lateral Distribution of Materials in the SEI Built on HOPG-TOF SIMS and XPS Studies. *J. Power Sources* **2001,** *97−98*, 52–57.
17. Naji, A.; Ghanbaja, J.; Humbert, B.; Willmann, P.; Billaud, D. Electroreduction of Graphite in LiClO4-Ethylene Carbonate Electrolyte. Characterization of the Passivating Layer by Transmission Electron Microscopy and Fourier-Transform Infrared Spectroscopy. *J. Power Sources* **1996,** *63*, 33–39.
18. Egerton, R. F.; Wang, F.; Crozier, P. A. Beam-Induced Damage to Thin Specimens in an Intense Electron Probe. *Microsc. Microanal.* **2006,** *12*, 65–71.
19. Egerton, R. F.; McLeod, R.; Wang, F.; Malac, M. Basic Questions Related to Electron-Induced Sputtering in the TEM. *Ultramicroscopy* **2010,** *110*, 991–997.
20. McKinley, W. A.; Feshback, H. The Coulomb Scattering of Relativistic Electrons by Nuclei. *Phys. Rev.* **1948,** *74*, 1759–1763.
21. Inokuti, M. Inelastic Collisions of Fast Charged Particles with Atoms and Molecules—The Bethe Theory Revisited. *Rev. Mod. Phys.* **1971,** *43*, 297–347.
22. Egerton, R. F.; Li., P; Malac, M. Radiation Damage in the TEM and SEM. *Micron* **2004,** *35*, 399–409.
23. Balasubramanian, M.; Johnson, C. S.; Cross, J. O.; Seidler, G. T.; Fister, T. T.; Stern, E. A.; Hamner, C.; Mariager, S. O. Fine Structure and Chemical Shifts in Nonresonant Inelastic x-ray Scattering from Li-Intercalated Graphite. *Appl. Phys. Lett.* **2007,** *91*, 031904(1−3).
24. Momose, H.; Honbo, H.; Takeuchi, S.; Nishimura, K.; Horiba, T.; Muranaka, Y.; Kozono, Y.; Miyadera, H. X-ray Photoelectron Spectroscopy Analyses of Lithium Intercalation and Alloying Reactions on Graphite Electrodes. *J. Power Sources* **1997,** *68*, 208–211.
25. Wertheim, G. K.; Vanattekum, P. M.; Th., M.; Basu, S. Electronic Structure of Lithium Graphite. *Solid State Commun.* **1980,** *33*, 1127–1130.
26. Grunes, L. A.; Gates, I. P.; Ritsko, J. J.; Mele, E. J.; Divicenzo, D. P.; Preil, M. E.; Fischer, J. E. Valence and Core Electronic Excitations in LiC_6. *Phys. Rev. B: Condens. Matter Mater. Phys.* **1983,** *28*, 6681–6686.
27. Hightower, A.; Ahn, C. C.; Fultz, B.; Rez, P. Electron Energy-Loss Spectrometry on Lithiated Graphite. *Appl. Phys. Lett.* **2000,** *77*, 238–240.
28. Song, X.; Kinoshita, K.; Tran, T. Microstructural Characterization of Lithiated Graphite. *J. Electrochem. Soc.* **1996,** *143*, L120–123.
29. Dresselhaus, M. S.; Dresselhaus, G. Intercalation Compound of Graphite. *Adv. Phys.* **1981,** *30*, 1–186.
30. Verma, P.; Maire, P.; Novak, P. A Review of the Features and Analyses of the Solid Electrolyte Interphase in Li-ion Batteries. *Electrochim. Acta* **2010,** *55*, 6332–6341.
31. Kanamura, K.; Tamura, H.; Takehara, Z. XPS Analysis of a Lithium Surface Immersed in Propylene Carbonate Solution Containing Various Salts. *J. Electroanal. Chem.* **1992,** *333*, 127–142.
32. Aurbach, D.; Zaban, A.; Ein-Eli, Y.; Weissman, I.; Chusid, O.; Markovsky, B.; Levi, M.; Levi, E.; Schechter, A.; Granot, E. Recent Studies on the Correlation between Surface Chemistry, Morphology, Three-Dimensional Structures and Performance of Li and Li-C Intercalation Anodes in Several Important Electrolyte Systems. *J. Power Sources* **1997,** *68*, 91–98.
33. Edstrom, K.; Herstedt, M.; Abraham, D. P. A New Look at the Solid Electrolyte Interphase on Graphite Anodes in Li-ion Batteries. *J. Power Sources* **2006,** *153*, 380–384.
34. Liu, D.; George Rommal, H. E.; Williams, D. B. Preparation of Lithium Specimens for Transmission Electron Microscopy. *J. Electron Microsc. Tech.* **1986,** *4*, 381–383.
35. Zenser, L. P.; Gruehn, R.; Liebscher, B. H. Decomposition of MgF2 in the Transmission Electron Microscope. *J. Solid State Chem.* **2001,** *157*, 30–39.
36. Hébert, C. Practical Aspects of Running the WIEN2k code for Electron Spectroscopy. *Micron* **2007,** *38*, 12–28.
37. Jorissen, K.; Rehr, J. J.; Verbeeck, J. Calculations of Electron Energy Lss and X-Ray Absorption Spectra in Periodic Systems without a Supercell. *Phys. Rev. B: Condens. Matter Mater. Phys.* **2010,** *81*, 155108(1−6).
38. Blaha, P.; Schwarz, K.; Madsen, G.; Kvasnicka, D.; Luitz, J. *WIEN2 K, An Augmented Plane Wave+Local Orbital Program for Calculating Crystal Properties*; Karlheinz Schwarz, Technical University: Wien, Austria, 2001.